Monte-Carlo simulation and analytical expressions for the extrapolated range and transmission rate of low energy electrons [10 eV -10 keV] in 11 monoatomic materials

Quentin Gibaru, Christophe Inguimbert, Mohamed Belhaj, Mélanie Raine, Damien Lambert

Monte-Carlo simulation and analytical expressions for the extrapolated range and transmission rate of low energy electrons [10 eV - 10 keV] in 11 monoatomic materials

Q. Gibaru[1,2,3], C. Inguimbert[1], M. Belhaj[1], M. Raine[2], D. Lambert[2]

[1]ONERA-DPHY, 2 avenue E. Belin, 31055 Toulouse, France
[2]CEA, DAM, DIF - 91297 ARPAJON, France
[3]CNES, 18 av. E. Belin, 31401 Toulouse CEDEX, France

Abstract—. The “extrapolated range” of electrons is a very practical physical parameter widely used in many applications. The commonly used analytical expressions are given classically for energies down to ~1 keV. Low energy Monte Carlo simulations have been performed to extract this parameter in various materials down to several tens of eV. These simulations have been used to parameter both, transmission probability and projected range analytical expressions. These empirical equations have been extended to 11 monoatomic elements (C, Be, Al, Si, Ti, Ni, Cu, Ge, Ag, Fe and W) and for energies ranging from ~10 eV up to some tens of MeV.

1 Introduction

The penetration distance of electrons in solid materials can be evaluated by the use of the extrapolated range, which can be derivated from the transmission probability [1,2]. The knowledge of this parameter is very useful to several fields related to electron beams, such as electron spectroscopy [3], which is based on high-resolution measurements of the characteristics of emitted electrons. These secondary electrons escape only from depths of a few nanometers, corresponding to energies down to a few tens of eVs. Thus, the range of low energy electrons is required for these surface analysis methods. The related secondary electron emission (SEE) process is also of capital importance in the performance of various devices [4,5], whose materials may be selected to increase or decrease the quantity of emitted electrons. For instance, in the field of space technologies, the multipactor phenomenon that may occur in Radio-Frequency (RF) components of satellites is driven by the SEE mechanism [6,7]. As a result, low SEE materials are required in order to prevent the triggering of this effect. In this context, the electron extrapolated range is a fundamental parameter commonly used in SEE yield models [8,9]. Accurate extrapolated range analytical expressions valid down to few eV for various materials is thus of great interest to improve the reliability of these SEE yield models. It could also be very helpful for analtyticaly based ionizing dose calculations.In addition, the extrapolated range formulas are often used as input parameters in higher simulation codes that models the interaction of plasma with surface or multipactor effect [10,11]

Several empirical formulas for the range of electrons are already available in the literature [12–22], most of them having been extrapolated from experimental data. However, for electron energies below 1 keV, experimental difficulties appear and make the evaluation of the extrapolated range relationship quite difficult. As a result, the low energy thresholds of the analytical expressions found in the literature [12–21] extend at best down to ~1 keV. But several applications, such as secondary electron emission [22] or surface analysis techniques, for instance electron spectroscopy [23], require models that are valid down to a few eVs.

In this scope, we propose here to use a Monte Carlo electron transport code to determine numerically the extrapolated ranges and transmission probabilities of electrons down to few tens of eVs. The MicroElec [24–26] module of GEANT4 [27] has been used for 11 materials, as a reference to extend the validity domain of the range/energy formula proposed by Weber [13–15]. For these materials, this formula now ranges from few tens of eV up to several tens of MeV. Moreover, as the extrapolated range for electrons of a given energy is dependent on the transmission probability of these electrons through a certain thickness, an analytical expression of this probability is also proposed in this work.

2 Definitions of the Range and extrapolated range

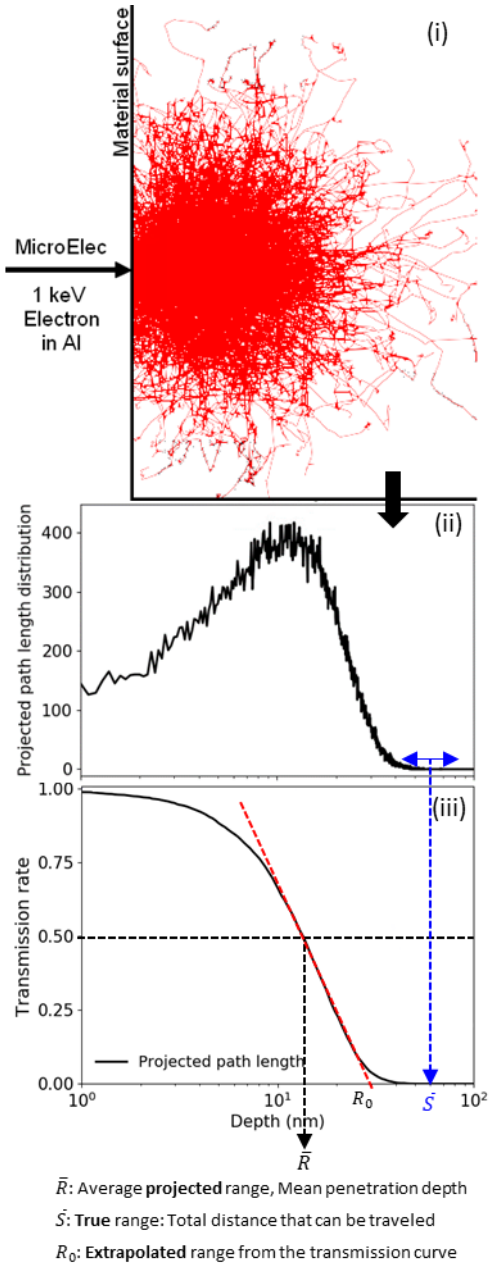

Figure 1: Definition of the true range and the projected range of electrons.

i. The trajectories of incident electrons are simulated.

ii. The final depths reached by incident electrons when coming at rest are extracted from the simulation and sampled as a depth distribution.

iii. The transmission rate and range are deduced from the distribution of depths.

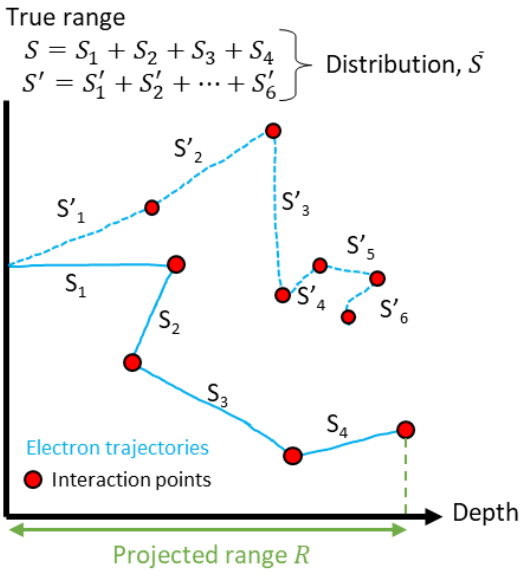

Figure 2: Definition of the true range and projected range from an electron's trajectory

When electrons penetrate in a material, they lose energy by inelastic interactions with electrons of the target atoms, and are slowed down by doing successive interactions. Electrons can also be highly scattered by the target atoms' nuclei. As a result, each particle has an individual trajectory, as seen on Figure 1 (i) and Figure 2.

The true range S of a given trajectory is the total distance traveled until the electron comes at rest, i.e. the sum of all step lengths S_i traveled by the particle between each interaction, as illustrated on Figure 2. This parameter can be sampled for a large number of electrons to get the average true range $\bar{S}$, which is an indication of the total distance traveled by the electrons in average. Within the Continuous-Slowing-Down Approximation (CSDA), $\bar{S}$ can be evaluated thanks to the following integral:

$$\bar{S}(E) = \int_0^E \frac{1}{dQ/dx} dQ \qquad (1)$$

This is the integral of the reciprocal of the stopping power (dQ/dx) over energy from a final to an initial value: It corresponds to the parameter $\bar{S}$ from the definition of Figure 2. The CSDA range is the total distance that is effectively travelled by electrons. However, $\bar{S}$ does not give information on the final position of the particles or in which direction they have traveled. But, the depth reached by the electrons depends, in addition to the slowing down induced by inelastic scattering, to the deviations generated by the inelastic and elastic interactions. In this regard, $\bar{S}$ can be interpreted as a penetration depth that can only be reached by a theoretical electron with a strictly linear trajectory. As this is never the case for electrons, which are deflected by elastic interactions, this parameter is an unreachable limit for the actual range R. Moreover, $\bar{S}$ is not accessible experimentally as the electrons do not behave in a deterministic way but follow statistical laws for each step.

In consequence, for many applications, the paths of the particles are expressed as a projection on the incident direction of the impinging particle, generally in the depth of the material. Thus, a more convenient method is to sample the final positions of electrons along this direction. This can be done following the method on Figure 2 to get the projected range R for a given trajectory. For instance, sampling the distribution of the final depths R reached by a large number of electron trajectories, as done on Figure 1 (ii), allows us to compute its average $\bar{R}$, which corresponds to the average of the depths reached by the electrons in a semi-infinite material.

In this paper, the penetration depth of an electron is defined as the final depth reached by the electron when it comes at rest. The transmission rate through a thickness d is thus defined as the proportion of electrons with a final position deeper than d.

For electrons, that are highly scattered, two other parameters can be found in the literature to describe their trajectories. The extrapolated range and the practical range are commonly evaluated.

The extrapolated range (R_0) is commonly defined following the method shown on Figure 1 (iii), taken as the point of intersection between the tangent at the steepest section of the transmission probability curve (P=0.5) and the depth axis (X-axis) [20,21]. In the following, the range value given by this point will be called R_0. Similarly, the practical range can be obtained from the depth-dose profile in place of the transmission curve. Both parameters are evaluated in slightly different ways, but have often been used interchangeably [28] as they remain similar. They differ in their definition from a simple average over the penetration depths from each individual trajectory, but are more representative of the penetration distance of individual electrons. Hence they are commonly used to define the shielding thickness necessary to protect an equipment from radiation.

In this work, we have chosen to use the extrapolated range defined from the transmission rate. At high energy (E>keV), the ranges of electrons are demonstrated to be independent on the nature of the target material, they are proportional to the density ρ (g/cm^3). For this reason, the range values are commonly expressed in g/cm² and normalised to the density as $R_0(E) * \rho$ (2).

Many empirical range-energy expressions have been proposed by several authors [12–21], describing the electron extrapolated ranges in various materials, aluminum being the most extensively studied material. Most of these relationships are in the form of a power law:

$$R_0(E) = k * E^n \quad (3)$$

Katz and Penfold [12] have made a very thorough compilation of experimental results for aluminum, and have proposed an empirical formula for the extrapolated range of electrons between 10 keV and 3 MeV. In this formula, widely used in the past, the *n* factor in equation (3) is a function of the energy of the electrons:

$$n = 1.265 - 0.0954 \ln(E) \quad (4)$$

With $R_0(E)$ in mg/cm², $k = 412$. Sometimes n also depends on the material [18]. Weber [13] proposed a different expression, valid for aluminum in the energy region [3 keV, 3 MeV].

Kobetich and Katz [14] extended this model to the 0.3 keV- 20 MeV range by adjusting the constants:

$$R_0(E) = AE\left[1 - \frac{B}{(1+CE)}\right] \quad (5)$$

where $R_0(E)$ is the extrapolated range, *E* the kinetic energy of the electrons,

$$A = 5.37 \cdot 10^{-4}\ g/cm^2/keV,\ B = 0.9815,$$
$$C = 3.123 \cdot 10^{-3}\ keV^{-1}. \quad (6)$$

The same authors [15] proposed further improvements for this formula, by introducing a dependence on the atomic number Z of the material for the three parameters:

$$A = (1.06 \cdot Z^{-0.38} + 0.18) \cdot 10^{-3}\ g/cm^2\,.keV$$
$$B = 0.22 \cdot Z^{-0.055} + 0.78$$
$$C = (1.1 \cdot Z^{0.29} + 0.21) \cdot 10^{-3}\ g/cm^2\,.keV \quad (7)$$

Most of the other models found in the literature suppose that the extrapolated range tends to zero by following a power law [16-21]. However, contrary to the Weber expression, they are not relevant on the whole energy range. The Weber expression has also the advantage of being able to either express the extrapolated range *x* as a function of the energy *E* or inversely *E* as a function of *x*.

This work proposes to improve the model of ref. [15] (equations (5) and (7)), and extend its low energy from a few keV to 10 eV.

3 Monte Carlo transportation code for low energy electrons

In this work, the MicroElec module of the Monte-Carlo simulation toolkit GEANT4 has

been used [26]. Many physical models are available in GEANT4 and can be sorted between continuous or discrete processes. Continuous processes can use continuous energy loss and multiple-scattering models for the slowing down and deviation of electrons, as opposed to discrete processes, which compute a specific energy loss and angular deviation of the electron for each single step. As a result, continuous processes are much faster in terms of computing time, especially at higher energies (>1 keV), but the increased accuracy of discrete processes is appreciable for low energy electrons (< 1keV) and data sampling on nanometric distances.

The MicroElec module, which we have developed, only uses discrete processes. It is intended for the transportation of low energy electrons down to a few eVs in 11 materials and has been validated for this purpose with experimental SEE Yield data. In the [eV - keV] energy range, electrons traveling in a solid interact with the atoms of the material and can be elastically scattered by the nuclei or inelastically scattered by the electrons. In this case, the main source of energy loss for the incident electrons are inelastic interactions with weakly bound and plasmon electrons.

The dielectric formalism, with Mermin's dielectric function, is used in MicroElec for individual and collective interactions with electrons of the conduction band, or valence band for insulators. The ionisation of core shells is also treated with this approach [29]. The implementation of the dielectric formalism has been validated with reference stopping power data [26]. Finally, the cross sections for the coulombian elastic interaction are computed with the ELSEPA code using the partial-wave method [30].

In the newly released version of MicroElec (GEANT4 10.7), the transportation of low energy electrons can be simulated in 11 materials, including 2 compound materials. However, the scope of this work is to extend the work of Kobetich & Katz [15], and thus derive analytical expressions for the extrapolated range and transmission probabilities that keep a relationship with the atomic number Z. Consequently, this paper only shows the simulation results for monoatomic materials, namely C, Al, Si, Ti, Ni, Cu, Ge, Ag and W. Simulations results are also shown for Be and Fe, these materials have been validated with experimental SEY data [31] but are yet to be released in GEANT4. 10000 events are simulated for a computation time of about 1 min for energies below 5keV. Since the secondary electron cascade is not simulated, the computation is much faster. All simulations have been performed in the case of a normal incidence beam on a flat semi-infinite surface.

The simulation results of MicroElec for these 11 materials have been used to define and parameterize an energy/range analytical formula and a transmission probability formula depending on the former expression. Both are relevant down to ~10 eV.

4 Monte-Carlo simulations

4.1 Transmission rate

First, the transmission rates should be computed as they will be needed to deduce the extrapolated range following the method described in section 2. The implantation depths for incident electrons between 25 eV and 5 keV have been sampled from MicroElec simulations and used to calculate the transmission probability as a function of the incident electron energy. They are shown in Figure 3 for beryllium, aluminium, iron and silver, which have respective densities of 1.85, 2.7, 7.87 and 10.5 g/cm².

At low energies, the penetration depths are comparable for all four materials, around 1-2 nanometers. However, as the energy increases, the penetration depths, expressed in nm on Figure 3, increase more quickly for low density materials. This effect is visible in Figure 3 as the transmission curves become less widespread when the material density increases. Indeed, for 2 keV electrons the

penetration depth can reach hundreds of nanometers in aluminum and beryllium, but only 40 nm in iron and silver. At very low energies, the penetration depth becomes about the order of the interatomic distances and the notion of a transmission rate becomes debatable. This discussion is detailed in section 6. The figures for the transmission rates of all 11 materials obtained from MicroElec can be found in Annex 2.

Moreover, the intervals between the transmission rate curves of all four materials become very small for electron energies below 100 eV. This implies that the extrapolated ranges extracted from these transmission curves should decrease more slowly below 100 eV, as will be studied in the next section.

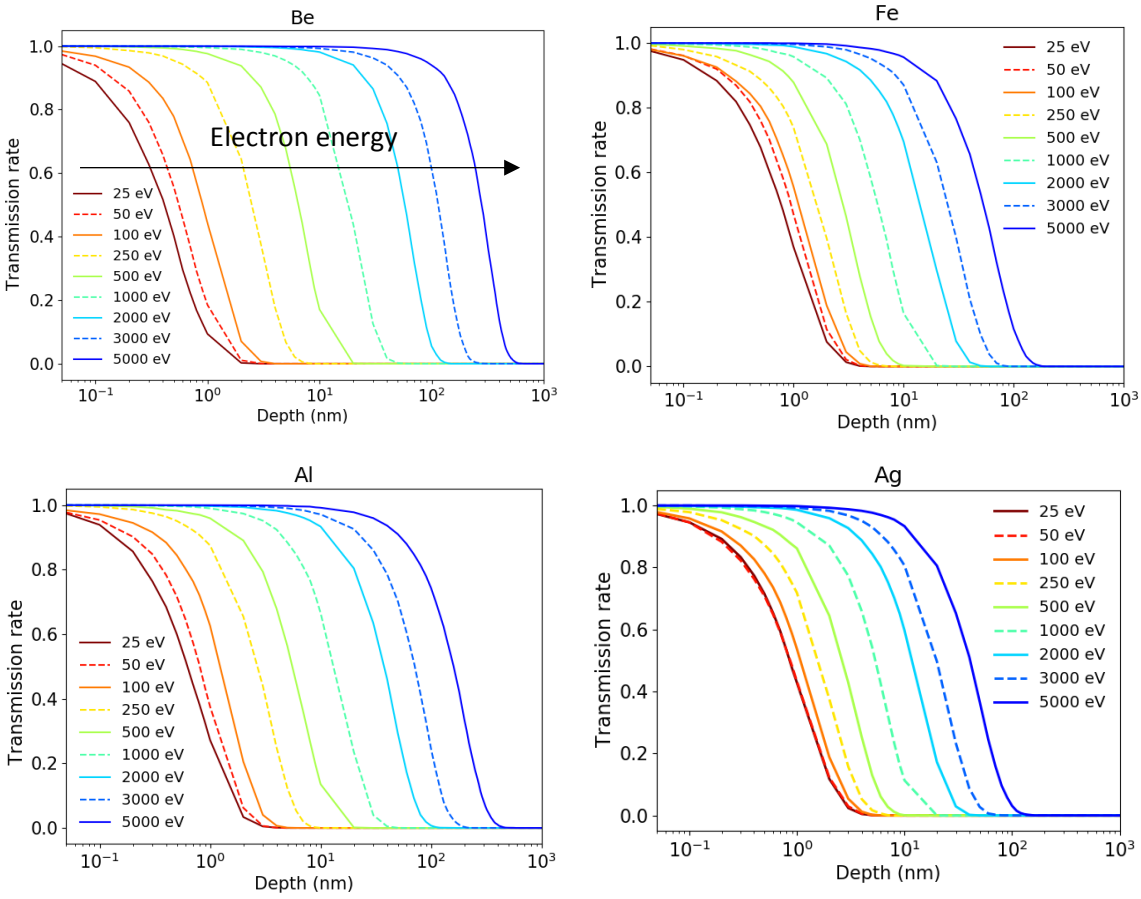

Figure 3: Electron transmission rate for Be, Al, Fe and Ag materials. The energy of electrons range from 25 eV up to 5 keV.

4.2 Extrapolated RANGE

In Figure 4 the extrapolated ranges (R_0) computed with MicroElec, which uses discrete processes, are compared with extrapolated range computations made with the continuous processes of GEANT4's standard physics list (Opt4) for aluminum and silicon. This physics list is designed for precise transportation of electrons on a wide range of energies. For energies under 10 keV, the PENELOPE continuous energy loss ionization model is used with a multiple scattering model for elastic interactions. Monte-Carlo simulated data from Colladant et al. [32], Akkerman et al. [28] and experimental data from Kanter & Sternglass [33] are also displayed, but the available experimental data for the extrapolated range of low energy electrons below 1 keV is very scarce. Finally, the range given by equations (5) and (7) (Weber

Formula), and the CSDA range ($\bar{S}$) obtained with eq. (1) from MicroElec's stopping powers (in green, labeled CSDA) for both materials are displayed on both figures.

The extrapolated range curves show a typical behavior below a few hundreds of eVs. They are no more proportional to the incident energy, and the range/energy function stabilizes as the range reaches a plateau region whose height depends on the material. This effect is more visible on the MicroElec curve and can also be seen on the CSDA curves computed from the MicroElec stopping powers, which become parallel to each other at lower energies. The level of this plateau region changes from a material to another as a function of the relative values of the inelastic and elastic mean free paths.

One can notice that, for both materials, the CSDA ranges ($\bar{S}$) obtained from eq. 1 with MicroElec's stopping powers converge to about 2 times the extrapolated range (R_0) obtained from MicroElec simulations. However, the CSDA gives values which are much higher than the simulated data sets below a few keV. This can be explained by the fact that the CSDA is a maximum range which neglects the deflection induced by the elastic and inelastic interactions, and would only be attained by a hypothetical electron with a strictly linear trajectory. As this is never the case for electrons, this parameter is an unreachable limit for the actual range R_0.

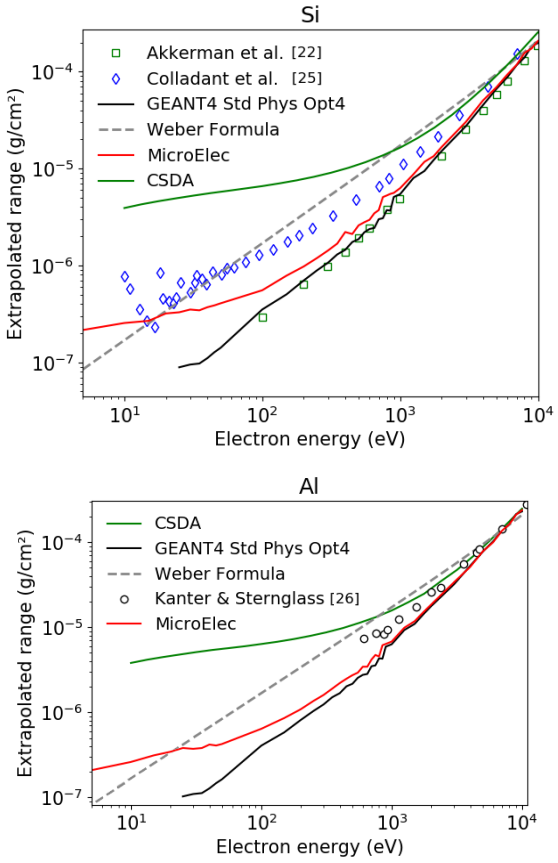

Figure 4:Extrapolated ranges of low energy electrons in Al and Si

Indeed, below 100 eV, the elastic scattering becomes prevalent over the inelastic scattering for electrons. This can be shown qualitatively by calculating the probability P_{El} that the interaction made by the electron is an elastic interaction. It is obtained from the total cross sections (TXS) as:

$$P_{El} = \frac{Elastic\ TXS}{Elastic\ TXS + Inelastic\ TXS} \qquad (12)$$

As can be seen on

Figure 5, P_{El} increases strongly below 50 eV, where energy losses become rarer, and approaches 1 below 20 eV. This behavior can also be seen for other Monte-Carlo codes, as mentioned by Pierron et al. [34].

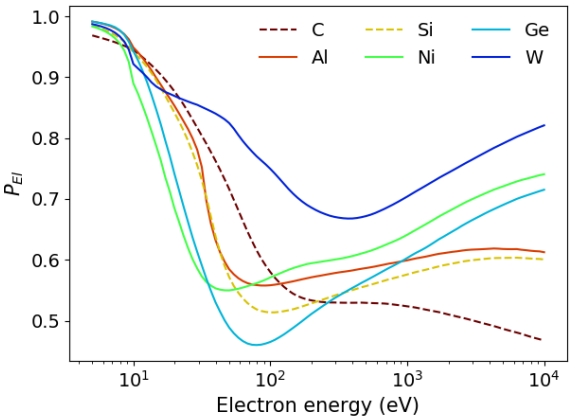

Figure 5:Elastic scattering ratio for 6 materials

Quantitatively, the elastic MFP becomes an order of magnitude lower than the inelastic MFP, with values of a few nanometers, as shown in Figure 6. Due to the divergence of the inelastic mean free path, the CSDA range also displays a flattening effect below 100eV.

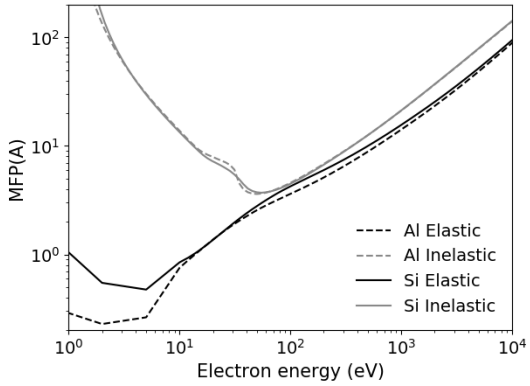

Figure 6: Mean free paths of electrons in MicroElec for Si and Al

But, as mentioned in section 2, this range is a maximum depth that will not be reached by most electrons. Indeed, at these energies the angular distribution of the elastic scattering becomes quasi-isotropic (Figure 1). Consequently, the transportation of low energy electrons below 50 eV becomes a case of random diffusion: they are highly scattered without any energy loss until an inelastic interaction occurs, then leading the particle to come at rest. Hence, the electron can travel a longer total path before being stopped, while remaining close to the surface.

However, we can see that the CSDA range, which does not take into account the elastic diffusion, becomes parallel with the extrapolated range at lower energies. This shows that the elastic interaction does not change the dynamic of the range. It only reduces the values of the projected range by diffusing the trajectories of the particles, and the intensity of this reduction becomes larger as the energy and elastic MFP decrease. Hence, the flattening dynamic could rather be caused by the divergence of the inelastic MFP.

The plateauing effect at very low energies does not seem to be reproduced by the GEANT4 continuous processes (Std Phys Opt4). Indeed, this physics package uses multiple scattering instead of discrete elastic models, which can also generate more differences. Above 1keV however, the GEANT4 continuous processes give similar values to MicroElec.

This behaviour can be linked with the transmission probabilities in Figure 7, in the example of silicon. The intervals between the transmission curves computed with MicroElec become narrower as the energy decreases, as seen for the other materials in Figure 3. However, the transmission curves obtained with the standard physics keep a spread of about the same order at lower and higher energies on the lin-log plot. This implies a linear (on a log-log plot) decrease of the extrapolated range for the whole energy range of 25 eV-10 keV seen in Figure 4. The comparison is given here as an indication of the differences which can occur at very low energies, when using different interaction models with different approaches (continuous vs discrete) and different mean free paths. We have already conducted a more extensive comparison between the different physics models of GEANT4, which can be found in ref. [35].

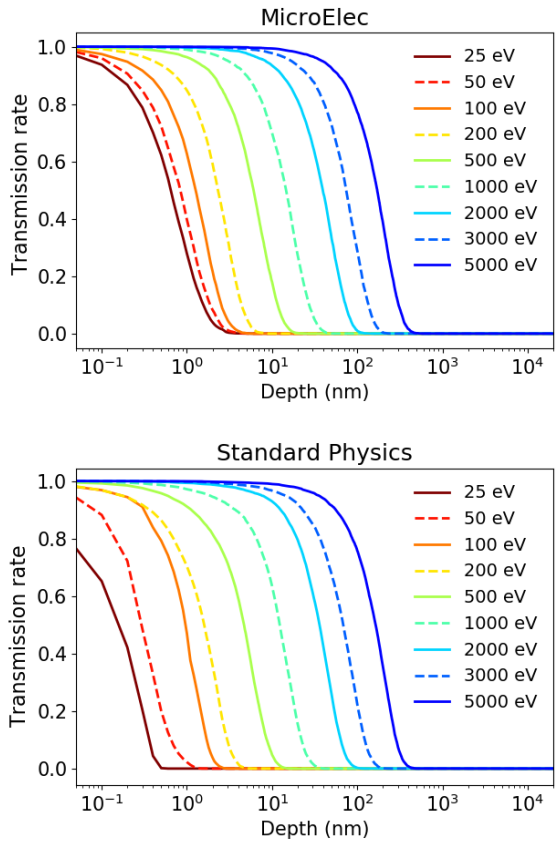

Figure 7: Comparison of the transmission rates in Si from MicroElec and the standard continuous processes

5 Analytical expressions

5.1 Extrapolated range expression

Above some keV, expression (3) reproduces faithfully the Monte-Carlo simulations and experimental data. However, the commonly used power law expressions are no longer applicable below 1 keV. As shown in Figure 3, equation (3) does not reproduce the dynamic of the extrapolated range below 1 keV, with a linear (log/log scale) evolution in place of the flattening phenomenon observed in the simulations. Thanks to the Monte Carlo simulations shown in the previous section 4, this expression has been modified in order to be relevant down to 10 eV. In our new expression, the model of ref. [15] is maintained for electron energies over 14.5 keV, as it is able to correctly model the dynamic of the range over this energy. This energy correspond to the points where our new expression best fit the formula of ref. [15]. Below this threshold, a power law function replaces the expression of the extrapolated range $r(E)$:

$$R_0(E) = \begin{cases} D(E+E_r)^F : 10eV < E \leq 14.5keV \\ AE\left[1-\frac{B}{(1+CE)}\right] : E \geq 14.5keV \end{cases} \quad (14)$$

With the following parameters:

$R_{0,Al} = 3 \cdot 10^{-7}\, g/cm^2$ is the extrapolated range of 50 eV electrons in aluminum obtained from the MicroElec simulations,

$$E_0 = 14.5\ keV$$

$$A = (1.06 \cdot Z^{-0.38} + 0.18) \cdot 10^{-3}\, g/cm^2 .keV$$

$$B = 0.22 \cdot Z^{-0.055} + 0.78$$

$$C = (1.1 \cdot Z^{0.29} + 0.21) \cdot 10^{-3}\, g/cm^2 .keV$$

$$E_r = \frac{E_0}{\left(\frac{AE_0\left[1-\frac{B}{(1+CE_0)}\right]}{G \cdot R_{0,Al}} - 1\right)^{\frac{1}{F}}}$$

$$D = \frac{AE_0\left[1-\frac{B}{(1+CE_0)}\right]}{(E_0+E_r)^F}$$

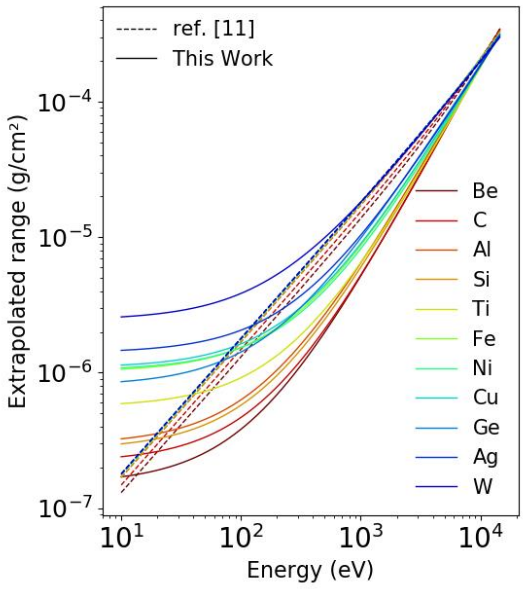

Figure 8: Comparison between the range models of eq. 5 and 13

As shown in Figure 8, above ~10 keV, the proposed new expression converges to the

classical formula provided by Weber [11]. Below this limit, the different extrapolated range expressions diverge. The new formulation reproduces the plateau region appearing in MC simulations while the former formula cannot mimic this behavior. This formula is compared with the Monte-Carlo simulations for all simulated materials in Figure 9(a) and 9(b).

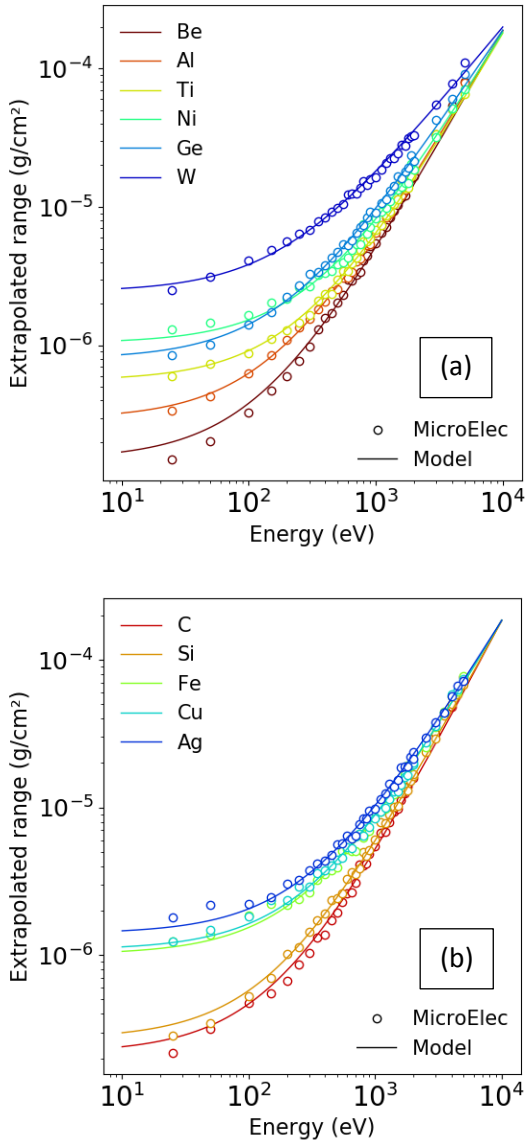

Figure 9: Comparison of the extrapolated ranges given by eq. 13 and MicroElec for all 11 materials (Be, Al, Ti, Ni, Ge and W in fig (a) and C, Si, Fe, Cu and Ag in fig (b))

Although the range below 50 eV is over estimated and the agreement with the simulations is decreased for low Z (Be, C) and high Z (W) materials, overall a satisfying agreement with the simulations is observed. Indeed, below 100eV, the average difference between the model and the simulation is between 3% and 12% for all materials, except for Be with 18%.

As can be seen on the comparison with the Weber formula in Figure 8, the new model shown in this work converges to the model of ref. [15] at 14.5keV and improves the range dynamic at lower energies.

The parameters of the model F and G are specific for each material and are determined with the following calibration process. The values of F and G are provided in the annex.

Aluminum, which is by far the more documented material, will serve as reference in the rest of the work. $G(Z)$ sets the height of the plateau region of the range curve for the material Z, relatively to the extrapolated range of 50 eV electrons in aluminum. It is defined as

$$G(Z) = \frac{\mathrm{R_{0,Z}}(50\ eV)}{R_{0,Al}} \quad (15)$$

With $R_{0,Z}(50eV)$ the extrapolated range of 50 eV electrons in the material Z. The values for $R_{0,Z}$ can be extracted from the Monte Carlo simulations. They are more representative of the actual differences between the ranges of the materials and give a better estimation of G. The ranges shown in Figure 9 use the G values from the simulations.

But, G can also be extracted from the ranges available in the literature. Though for energies this low, most available data are CSDA ranges which are not representative of the random walk of electrons. However, this data is available for many materials, like in the case of the stopping powers of Shinotsuka [36] that can be used to get the CSDA range and G parameter for 41 materials. Moreover, the dynamic of the CSDA range is similar to the one of the extrapolated range, as shown in Figure 4, due to the divergence of the inelastic

mean free paths which strongly increase below a few tens of eVs.

The $F(Z)$ factor defines the slope of the extrapolated range $dR_0(E)/dE$ between 1 and 10 keV, so that the curve reproduces the dynamic of the reference ranges.

The values for F and G in both cases are shown in Table ***1*** of the annex. In the case of the CSDA values, one must use $R_{0,Al} = 9 \cdot 10^{-7}\, g/cm^2$.

Figure 10 shows the correlation between the values of G(Z) and F(Z) for each material with the atomic number of the material Z. The strong correlation on fig. 9a shows that the height of the plateau region for a material is strongly dependent on the atomic properties of the material. Indeed, the range of low energy electrons below 100 eV tends to be higher in high Z materials, as shown on Figure 8. However, it is not trivial to provide a definite explanation for this correlation. At low energies, many properties depending on the Z or the material may influence the height of the plateau region, such as the number of conduction electrons per atom. This number is lower in Cu and Ag than for neighboring metals which could explain why their G values are slightly lower than expected. We can also observe that both Si and Ge have lower plateau heights than other materials with a close Z. We could then suppose that this discrepancy is due to the fact that these materials have an energy gap, which plays an important role in the energy loss process. Thus it is difficult to conclude on the origins of this dependence on Z and the observed discrepancies for some materials, and a more extensive study would be required.

Fig. 10b shows a more limited correlation between the slope of the range curve (F) and the atomic number, as F varies in a narrower range than G. This correlation is rather given as a starting point to extrapolate the parameter F and extend the model to other materials than the 11 shown here, which can also be done for G using the correlation relationship between Z and G.

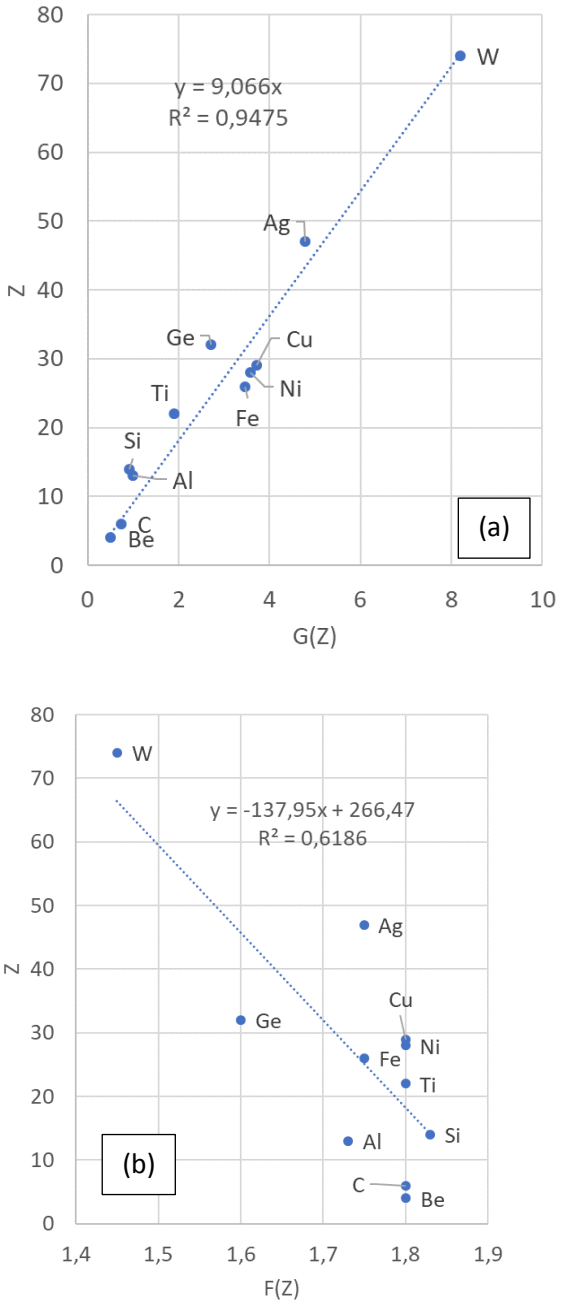

Figure 10: Correlation of the height of the range plateau (a) and the slope of the range curve (b) with the atomic number

5.2 Transmission rate expression

Analytical expressions have also been proposed for the transmission rate of electrons through a given thickness. But they are generally valid only for energies down to a few keV. As in the case of the extrapolated range, the probabilities calculated with MicroElec in section 4 can be used to calibrate

a new expression that is valid down to a few eV and suitable for SEY modelling. In this work, the model from Kobetick & Katz [15] has been extended to lower energies (~10 eV).

Their formula of the transmission probability $\eta(E,h)$ for electrons of energy E [keV] through a thickness h [g/cm^2], is initially given as a function of the extrapolated range $R_0(E)$ [g/cm^2]. In this case, the extrapolated range is obtained with the analytical expression shown in equation (3):

$$\eta(E,h) = e^{-\left(\frac{qh}{R_0(E)}\right)^p},$$
$$q = 0.0059\,Z^{0.98} + 1.1, \qquad (16)$$
$$R_0(E) = AE\left[1 - \frac{B}{(1+CE)}\right],$$
$$p = 1.8\,(\log_{10} Z)^{-1} + 0.31$$

This probability follows an exponential downward curve, whose parameters have been adjusted to get a satisfying agreement with our Monte Carlo simulations down to ~10 eV for the 11 materials. The new formula for the transmission probability uses the improved expression of the extrapolated range shown in section 5.1 below 14.5 keV. It is given for an energy E in MeV as:

$$\eta(E,h) = e^{-\left(\frac{qh}{R_0(E)}\right)^p}$$
$$R_0(E) = D(E+E_r)^F, \qquad (17)$$
$$\begin{cases} E \geq 2\ \text{keV} : p = 1.6 + 1.772\,e^{(-0.04Z)^{2/3}} \\ \qquad q = -0.0022\ \text{Z} + 1.6 \\ E < 2\ \text{keV} : p = \dfrac{\left(1.772\,e^{(-0.04Z)^{2/3}} - 0.12\right)}{2\ \text{keV}}E + 1.1 \\ \qquad q = -0.0022\ \text{Z} + 1.44 \end{cases}$$

The dependency in E in the expression of q has been added to take into account the flattening of the extrapolated range at lower energies. Indeed, with a simple numerical value, a compromise has to be made between the agreement with lower or higher energy curves. This dependency in E allows the model to better reproduce the varying spread of the transmission curves over a greater range of energies.

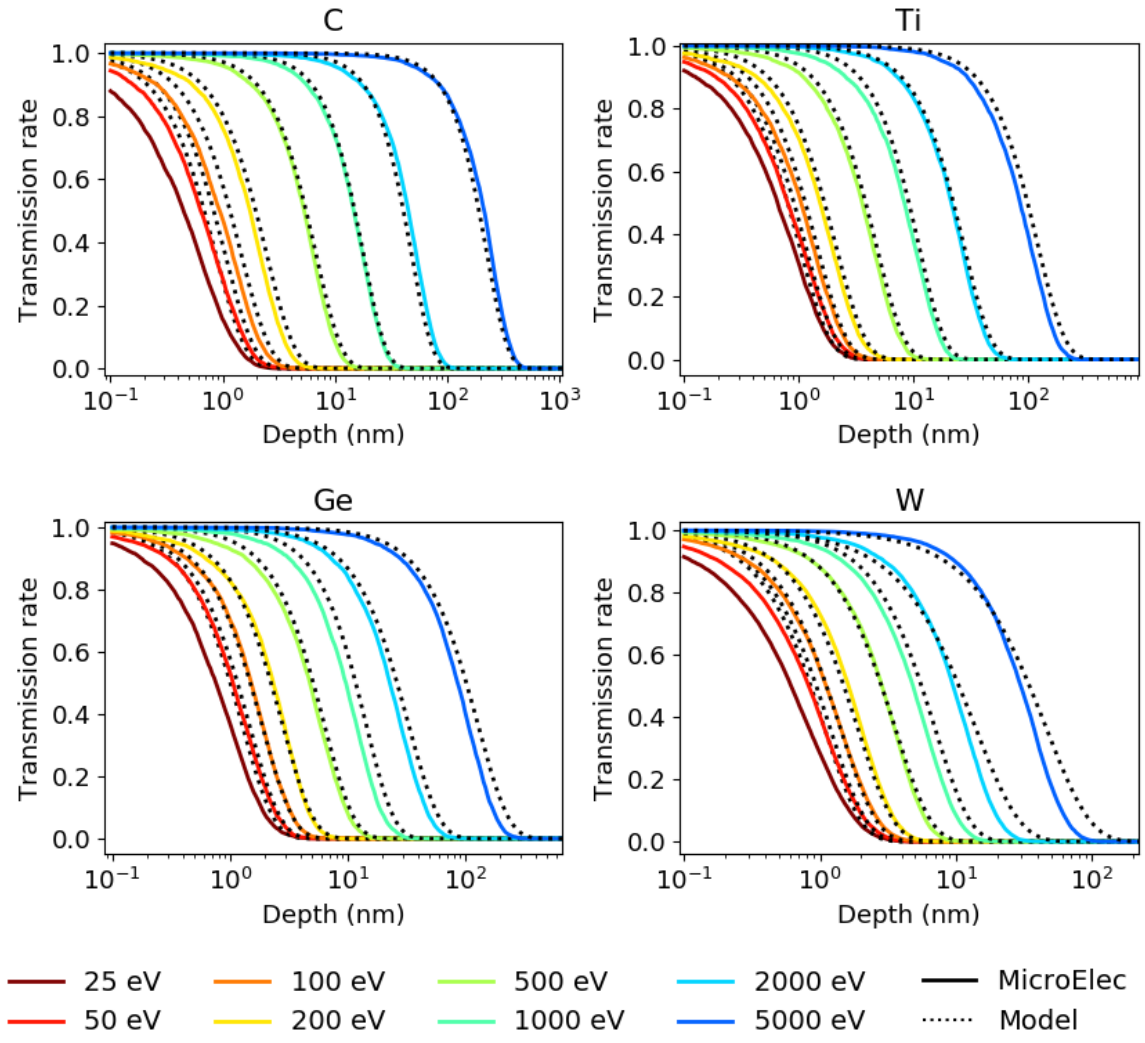

Figure 11: Transmission rate model (grey) compared with MicroElec (colors)

Figure 11 shows the comparison of the analytical model with the full Monte Carlo simulations in carbon, titanium, germanium and tungsten. The comparison between the analytical model and MicroElec for all 11 materials can be found in Annex 2. As in the case of the extrapolated range, a satisfying agreement is seen between the model and the simulations, although the agreement is degraded for very low and high Z materials (in the case of Be and W), and very low energies below 20 eV.

6 Discussion: Limits at very low energies

At very low energies and for low projected path lengths, the notion of an average range and a transmission probability becomes debatable. Indeed, at higher energies, many inelastic interactions can be made by the electrons in a unit path length dx. As shown on Figure 1, the ranges of electrons follow a Gaussian distribution with a well-defined average range and a limited spread. A single value of the range can thus be extrapolated and be used as a representative parameter for an individual electron. When the electron energies become very low, their projected path lengths reach the interatomic distances, they are highly scattered by the elastic interactions and they are only able to make a couple of inelastic interactions before coming at rest. Subsequently, the number of interactions made per unit path length dx is very small and the projected path length

distribution has a significant spread. Crucially, the depths reached by very low energy electrons become close to the interatomic distances (a few angstroms), which is another limitation for the number of interactions. The notion of a continuous function for the transmission probability through a few atomic layers may also become debatable. Finally, the Monte-Carlo code itself reaches its limits for very low depths and energies. Indeed, the material cannot be treated as a bulk material anymore and the use of the dielectric function theory as in the case of a bulk material is questionable.

To sum up, while the ranges and transmission rates evaluated at high energy are representative of the average path for an individual electron through a unit path length dx, the same extrapolation cannot be made at low energies where these quantities become statistical. Instead of an average electron, these parameters are applicable to a flux of a large number of electrons, where the global range and transmission rate of the flux should follow the models detailed in this work. An analogy can be made with the case of photons going through a certain thickness. A photon is fully absorbed by the material at the first interaction it makes, as in the case of very low energy electrons. Consequently, the transmission probability derived for photons is not representative of the path of each individual photon but of the flux of photons as a whole.

7 Conclusion

Monte-Carlo simulations of the penetration depths of electrons have been performed for 11 materials and used to compute the transmission rates and extrapolated ranges of electrons. An analytic formula for each of these two quantities is proposed, depending on the atomic number and two parameters that are specific for each material. The simulation results have been used to calibrate these expressions. While the analytical expression of the range does not strictly reproduce the simulation results at very low energies (< 50eV), it should be kept in mind that the range at these energies depends heavily on the mean free paths used. And, at very low energy, typically below the plasmon energy, the MFP calculation is subject to quite important uncertainties. The dielectric function theory, applied in our case reaches its limit which can be a significant limitation of the approach in the range of the very low energy limit. The computation also depends heavily on the elastic cross sections, which can have important uncertainities for very low energy electrons. As a result, some discrepancies can be observed depending on the mean free paths used by the different Monte Carlo codes, as in the case of Figure 4. Moreover, below ~10-20 eV, the transportation of electrons in matter is a random walk motion, and in this case, the definition of a representative mean range may become questionable. As a conclusion, and taking into account all these elements, the domain of validity of the analytical expressions proposed in this work for 11 monatomic materials (C, Be, Al, Si, Ti, Ni, Cu, Ge, Ag, Fe and W) can be considered to span from about 10-20 eV to 14.5 keV with a satisfying agreement with our Monte-Carlo code in this energy region.

A correlation for the material-dependent parameters F and G can be established with the atomic number Z. In the case of the plateau height G, a fairly strong correlation has been found, indicating that the behavior of very low energy electrons (below 100eV) is strongly dependent on the atomic properties of the material. These correlation laws can be used to extend the model to new materials. For the range-energy relationship a fairly good reproducibility should be obtained for new materials, even if non-metallic materials such as Si or Ge may have a slightly lower plateau height than expected. For the transmission probability model, the accuracy can be decreased for lower Z and higher Z materials

but a satisfying agreement can be expected in the intermediate region.

Finally, the analytical expressions can be of interest in other applications, such as higher level simulation codes which require the knowledge of the penetration depths of electrons in matter as input parameters. The analytical expressions of this work can thus be integrated in these simulation codes by their users, instead of interfacing their application with a Monte-Carlo simulation tool. In result, the analytical expressions would save computation time and make the code less complicated.

Another possible application would be to combine the expressions shown in this work to derive more analytical expressions for the ionizing dose deposited by low energy electrons. This approach will be presented in future work.

8 Acknowledgements

The authors would like to thank ONERA, CNES and CEA for providing the financial support for this work.

9 References

[1] W. Rall, The atomic nucleus. Robley Evans. McGraw Hill Book Company, Inc., New York (1955). 972 pp., $14.50, AIChE Journal. 2 (1956) 11S-12S. https://doi.org/10.1002/aic.690020327.

[2] CNES, ed., Radiation Environment and its effects on Spacecraft Components and Systems - COLLOQUE CNES SREC 04, Cépaduès éd., Toulouse, 2004.

[3] H. Seiler, Secondary electron emission in the scanning electron microscope, Journal of Applied Physics. 54 (1983) R1–R18. https://doi.org/10.1063/1.332840.

[4] K. Ohmi, Beam-Photoelectron Interactions in Positron Storage Rings, Phys. Rev. Lett. 75 (1995) 1526–1529. https://doi.org/10.1103/PhysRevLett.75.1526.

[5] N. Balcon, D. Payan, M. Belhaj, T. Tondu, V. Inguimbert, Secondary Electron Emission on Space Materials: Evaluation of the Total Secondary Electron Yield From Surface Potential Measurements, IEEE Transactions on Plasma Science. 40 (2012) 282–290. https://doi.org/10.1109/TPS.2011.2172636.

[6] J. Puech, E. Sorolla, J. Sombrin, M. Belhaj, P. Mader, J. Sinigaglia, Multipactor effect within RF dielectric components, Mulcopim. (2017).

[7] N. Fil, M. Belhaj, J. Hillairet, J. Puech, Multipactor threshold sensitivity to total electron emission yield in small gap waveguide structure and TEEY models accuracy, Physics of Plasmas. 23 (2016) 123118. https://doi.org/10.1063/1.4972571.

[8] G.F. Dionne, Effects of secondary electron scattering on secondary emission yield curves, Journal of Applied Physics. 44 (1973) 5361–5364. https://doi.org/10.1063/1.1662156.

[9] G.F. Dionne, Origin of secondary-electron-emission yield-curve parameters, Journal of Applied Physics. 46 (1975) 3347–3351. https://doi.org/10.1063/1.322061.

[10] C. Vicente, Multipactor and corona discharge: Theoretical fundamentals and analysis with CST and SPARK3D software tools, 2017 IEEE International Symposium on Electromagnetic Compatibility & Signal/Power Integrity (EMCSI). (2017). https://doi.org/10.1109/ISEMC.2017.8078121.

[11] J.-F. Roussel, F. Rogier, G. Dufour, J.-C. Mateo-Velez, J. Forest, A. Hilgers, D. Rodgers, L. Girard, D. Payan, SPIS Open-Source Code: Methods, Capabilities, Achievements, and Prospects, IEEE Transactions on Plasma Science. 36 (2008) 2360–2368. https://doi.org/10.1109/TPS.2008.2002327.

[12] L. Katz, A.S. Penfold, Range-Energy Relations for Electrons and the Determination of Beta-Ray End-Point Energies by Absorption, Rev. Mod. Phys. 24 (1952) 28–44. https://doi.org/10.1103/RevModPhys.24.28.

[13] K.-H. Weber, Eine einfache reichweite-energie-beziehung für elektronen im energiebereich von 3 keV bis 3 MeV, Nuclear Instruments and Methods. 25 (1963) 261–264. https://doi.org/10.1016/0029-554X(63)90196-4.

[14] E.J. Kobetich, R. Katz, Energy Deposition by Electron Beams and Delta Rays, Phys. Rev. 170 (1968) 391–396. https://doi.org/10.1103/PhysRev.170.391.

[15] E.J. Kobetich, R. Katz, Electron energy dissipation, Nuclear Instruments and Methods. 71 (1969) 226–230. https://doi.org/10.1016/0029-554X(69)90019-6.

[16] C. Feldman, Range of 1-10 kev Electrons in Solids, Phys. Rev. 117 (1960) 455–459. https://doi.org/10.1103/PhysRev.117.455.

[17] B.N. Subba Rao, A simple formula for the transmission and absorption of monoenergetic electrons, Nuclear Instruments and Methods. 44 (1966) 155–156. https://doi.org/10.1016/0029-554X(66)90456-3.

[18] T. Tabata, R. Ito, S. Okabe, Generalized semiempirical equations for the extrapolated range of electrons, Nuclear Instruments and Methods. 103 (1972) 85–91. https://doi.org/10.1016/0029-554X(72)90463-6.

[19] T. Tabata, P. Andreo, K. Shinoda, An analytic formula for the extrapolated range of electrons in condensed materials, Nuclear Instruments and Methods in Physics Research Section B: Beam Interactions with Materials and Atoms. 119 (n.d.) 463–470.

[20] T. Tabata, V. Moskvin, P. Andreo, V. Lazurik, Y. Rogov, Extrapolated ranges of electrons determined from transmission and projected-range straggling curves, Radiation Physics and Chemistry. 64 (2002) 161–167. https://doi.org/10.1016/S0969-806X(01)00469-8.

[21] D. Tan, B. Heaton, Simple empirical relations for electron CSDA range and electron energy loss, Applied Radiation and Isotopes. 45 (1994) 527–528. https://doi.org/10.1016/0969-8043(94)90120-1.

[22] J. Cazaux, A new model of dependence of secondary electron emission yield on primary electron energy for application to polymers, J. Phys. D: Appl. Phys. 38 (2005) 2433–2441. https://doi.org/10.1088/0022-3727/38/14/020.

[23] G.C. Smith, Surface Analysis by Electron Spectroscopy, in: G.C. Smith (Ed.), Surface Analysis by Electron Spectroscopy: Measurement and Interpretation, Springer US, Boston, MA, 1994: pp. 3–14. https://doi.org/10.1007/978-1-4899-0967-1_2.

[24] A. Valentin, M. Raine, J.-E. Sauvestre, M. Gaillardin, P. Paillet, Geant4 physics processes for microdosimetry simulation: Very low energy electromagnetic models for electrons in silicon, Nuclear Instruments and Methods in Physics Research Section B: Beam Interactions with Materials and Atoms. 288 (2012) 66–73. https://doi.org/10.1016/j.nimb.2012.07.028.

[25] M. Raine, M. Gaillardin, P. Paillet, Geant4 physics processes for silicon microdosimetry simulation: Improvements and extension of the energy-range validity up to 10 GeV/nucleon, Nuclear Instruments and Methods in Physics Research Section B: Beam Interactions with Materials and Atoms. 325 (2014) 97–100. https://doi.org/10.1016/j.nimb.2014.01.014.

[26] Q. Gibaru, C. Inguimbert, P. Caron, M. Raine, D. Lambert, J. Puech, Geant4 physics processes for microdosimetry and secondary electron emission simulation: Extension of MicroElec to very low energies and 11 materials (C, Al, Si, Ti, Ni, Cu, Ge, Ag, W, Kapton and SiO2), Nuclear Instruments and Methods in Physics Research Section B: Beam Interactions with Materials and Atoms. 487 (2021) 66–77. https://doi.org/10.1016/j.nimb.2020.11.016.

[27] J. Allison, K. Amako, J. Apostolakis, P. Arce, M. Asai, T. Aso, E. Bagli, A. Bagulya, S. Banerjee, G. Barrand, B.R. Beck, A.G. Bogdanov, D. Brandt, J.M.C. Brown, H. Burkhardt, Ph. Canal, D. Cano-Ott, S. Chauvie, K. Cho, G.A.P. Cirrone, G. Cooperman, M.A. Cortés-Giraldo, G. Cosmo, G. Cuttone, G. Depaola, L. Desorgher, X. Dong, A. Dotti, V.D. Elvira, G. Folger, Z. Francis, A. Galoyan, L. Garnier, M. Gayer, K.L. Genser, V.M. Grichine, S. Guatelli, P. Guèye, P. Gumplinger, A.S. Howard, I. Hřivnáčová, S. Hwang, S. Incerti, A. Ivanchenko, V.N. Ivanchenko, F.W. Jones, S.Y. Jun, P. Kaitaniemi, N. Karakatsanis, M. Karamitros, M. Kelsey, A. Kimura, T. Koi, H. Kurashige, A. Lechner, S.B. Lee, F. Longo, M. Maire, D. Mancusi, A. Mantero, E. Mendoza, B. Morgan, K. Murakami, T. Nikitina, L. Pandola, P. Paprocki, J. Perl, I. Petrović, M.G. Pia, W. Pokorski, J.M. Quesada, M. Raine, M.A. Reis, A. Ribon, A. Ristić Fira, F. Romano, G. Russo, G. Santin, T. Sasaki, D. Sawkey, J.I. Shin, I.I. Strakovsky, A. Taborda, S. Tanaka, B. Tomé, T. Toshito, H.N. Tran, P.R. Truscott, L. Urban, V. Uzhinsky, J.M. Verbeke, M. Verderi, B.L. Wendt, H. Wenzel, D.H. Wright, D.M. Wright, T. Yamashita, J. Yarba, H. Yoshida, Recent developments in Geant4, Nuclear Instruments and Methods in Physics Research Section A: Accelerators, Spectrometers, Detectors and Associated Equipment. 835 (2016) 186–225. https://doi.org/10.1016/j.nima.2016.06.125.

[28] A. Akkerman, M. Murat, J. Barak, Monte Carlo calculations of electron transport in silicon and related effects for energies of 0.02–200 keV, Journal of Applied Physics. 106 (2009) 113703. https://doi.org/10.1063/1.3256195.

[29] N.D. Mermin, Lindhard Dielectric Function in the Relaxation-Time Approximation, Phys. Rev. B. 1 (1970) 2362–2363. https://doi.org/10.1103/PhysRevB.1.2362.

[30] F. Salvat, A. Jablonski, C.J. Powell, ELSEPA—Dirac partial-wave calculation of elastic scattering of electrons and positrons by atoms, positive ions and molecules, Computer Physics Communications. 165 (2005) 157–190. https://doi.org/10.1016/j.cpc.2004.09.006.

[31] Q. Gibaru, C. Inguimbert, M. Belhaj, M. Raine, Low energy electrons Monte Carlo ionizing dose calculations and analytical expression for 11 materials, Submitted to Applied Surface Science. (n.d.).

[32] T. Colladant, A. L'Hoir, J.E. Sauvestre, O. Flament, Monte-Carlo simulations of ion track in silicon and influence of its spatial distribution on single event effects, Nuclear Instruments and Methods in Physics Research Section B: Beam Interactions with Materials and Atoms. 245 (2006) 464–474. https://doi.org/10.1016/j.nimb.2005.11.144.

[33] H. Kanter, E.J. Sternglass, Interpretation of Range Measurements for Kilovolt Electrons in Solids, Phys. Rev. 126 (1962) 620–626. https://doi.org/10.1103/PhysRev.126.620.

[34] J. Pierron, C. Inguimbert, M. Belhaj, M. Raine, J. Puech, Ionizing Doses Calculations for Low Energy Electrons in Silicon and Aluminum, IEEE Trans. Nucl. Sci. (2017) 1–1. https://doi.org/10.1109/TNS.2017.2662220.

[35] C. Inguimbert, P. Caron, Q. Gibaru, A. Sicard, N. Balcon, R. Ecoffet, Surface ionizing dose for space applications estimated with low energy spectra going down to hundreds of eV, IEEE Transactions on Nuclear Science. (2020) 1–1. https://doi.org/10.1109/TNS.2020.3045200.

[36] H. Shinotsuka, S. Tanuma, C.J. Powell, D.R. Penn, Calculations of electron stopping powers for 41 elemental solids over the 50eV to 30keV range with the full Penn algorithm, Nuclear Instruments and Methods in Physics Research Section

B: Beam Interactions with Materials and Atoms. 270 (2012) 75–92. https://doi.org/10.1016/j.nimb.2011.09.016.

ANNEX 1 : F and G parameters of the extrapolated range expression

Table 1: G F parameters from the M-C simulations (bold red) and from CSDA ranges [36]

Z	G	F
3	0.06	1.776
4	**0.51**	**1.8**
6	**0.74**	**1.8**
11	0.09	1.719
12	0.4	1.714
13	**1**	**1.73**
14	**0.92**	**1.83**
19	0.2156	1.656
21	1.386	1.69
22	**1.91**	**1.8**
23	2.6026	1.657
24	2.9722	1.64
26	**3.46**	**1.75**
27	4.774	1.654
28	**3.58**	**1.8**
29	**3.72**	**1.8**
32	**2.71**	**1.6**
39	1.8018	1.624
41	5.1128	1.599
42	5.9444	1.594
44	6.1138	1.593
45	5.5748	1.599
46	5.0974	1.6
47	**4.78**	**1.75**
49	3.2648	1.601
50	4.1118	1.6
55	0.4928	1.599
74	**8.2**	**1.45**

Annex 2: Figures for the transmission rate analytical model of all materials

In this section the transmission probabilities given by the analytical for all materials are shown. The model curves (dotted lines) are compared with the transmission rate given by MicroElec (solid lines).

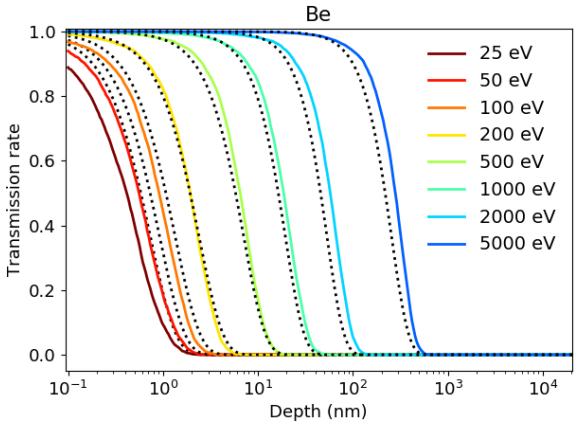
Be
Transmission rate
Depth (nm)
25 eV
50 eV
100 eV
200 eV
500 eV
1000 eV
2000 eV
5000 eV

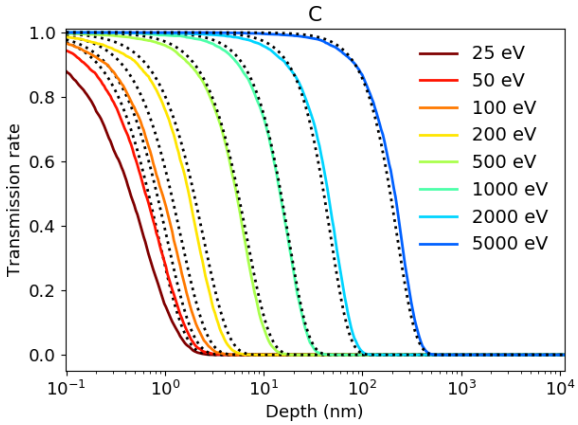
C
Transmission rate
Depth (nm)
25 eV
50 eV
100 eV
200 eV
500 eV
1000 eV
2000 eV
5000 eV

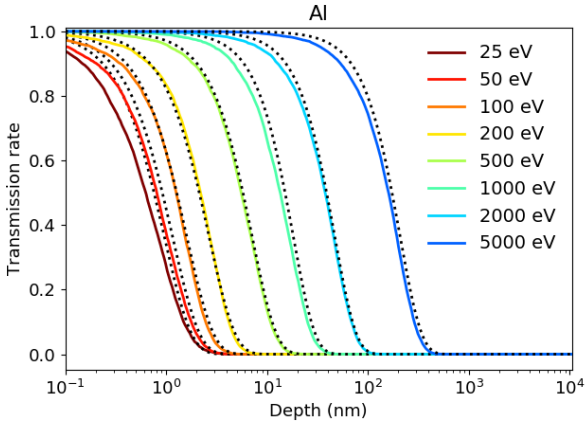
Al
Transmission rate
Depth (nm)
25 eV
50 eV
100 eV
200 eV
500 eV
1000 eV
2000 eV
5000 eV

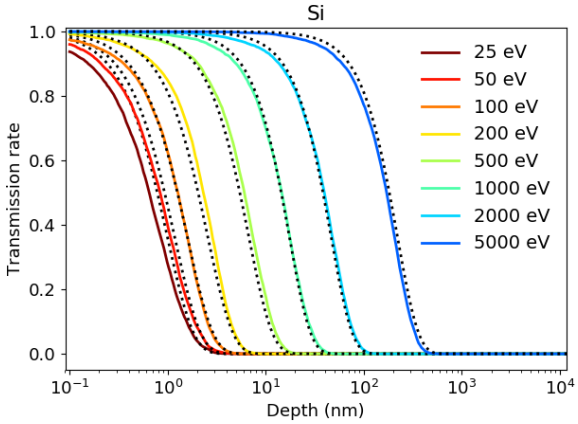
Si
Transmission rate
Depth (nm)
25 eV
50 eV
100 eV
200 eV
500 eV
1000 eV
2000 eV
5000 eV

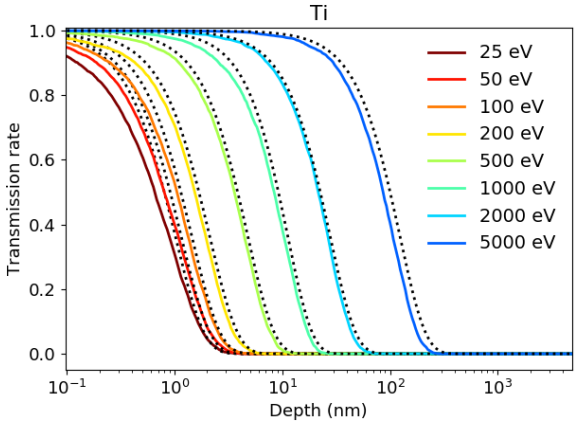
Ti
Transmission rate
Depth (nm)
25 eV
50 eV
100 eV
200 eV
500 eV
1000 eV
2000 eV
5000 eV

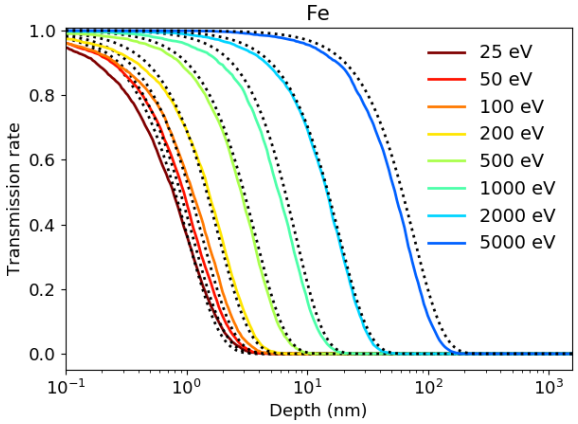
Fe
Transmission rate
Depth (nm)
25 eV
50 eV
100 eV
200 eV
500 eV
1000 eV
2000 eV
5000 eV

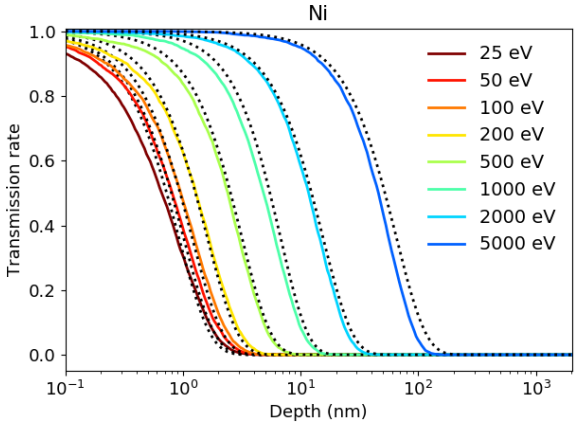
Ni
Transmission rate
Depth (nm)
25 eV
50 eV
100 eV
200 eV
500 eV
1000 eV
2000 eV
5000 eV

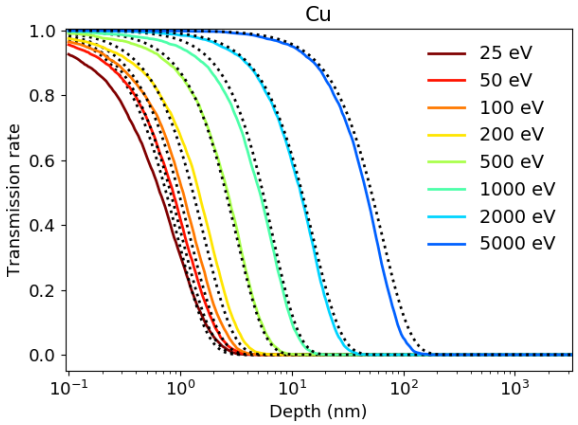
Cu
Transmission rate
Depth (nm)
25 eV
50 eV
100 eV
200 eV
500 eV
1000 eV
2000 eV
5000 eV

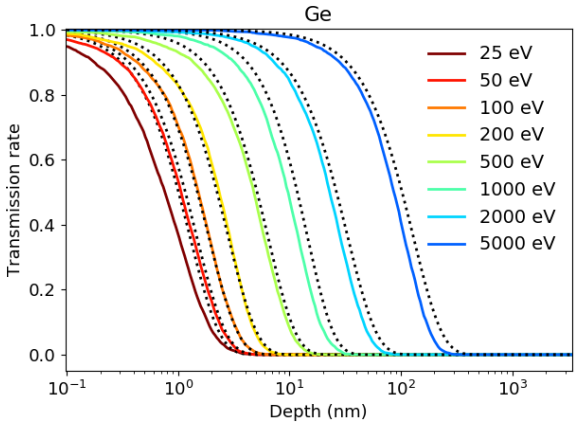
Ge
Transmission rate
Depth (nm)
25 eV
50 eV
100 eV
200 eV
500 eV
1000 eV
2000 eV
5000 eV

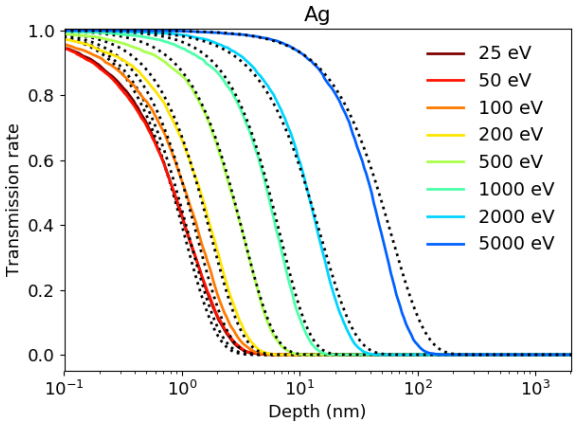
Ag
Transmission rate
Depth (nm)
25 eV
50 eV
100 eV
200 eV
500 eV
1000 eV
2000 eV
5000 eV

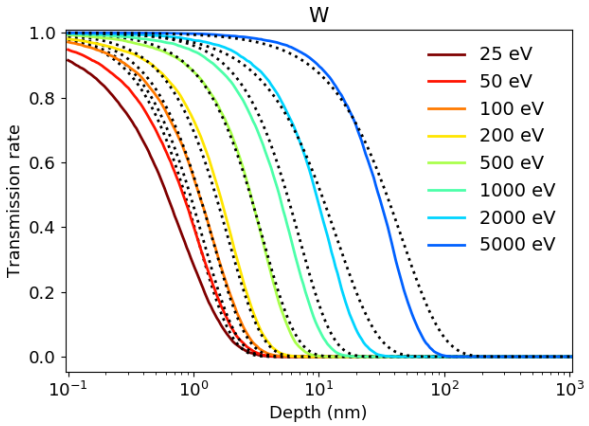
W
Transmission rate
Depth (nm)
25 eV
50 eV
100 eV
200 eV
500 eV
1000 eV
2000 eV
5000 eV